Published in final edited form as:
Nucl Med Biol. 2013 February ; 40(2): 289–294. doi:10.1016/j.nucmedbio.2012.11.004.

Evaluation of [^{18}F]Nifene biodistribution and dosimetry based on whole-body PET imaging of mice

Cristian C. Constantinescu, **Adriana Garcia**, **M Reza Mirbolooki**, **Min-Liang Pan**, and **Jogeshwar Mukherjee**
Preclinical Imaging, Department of Radiological Sciences, University of California Irvine, Irvine, CA 92697

Abstract

Introduction—[^{18}F]Nifene is a novel radiotracer specific to the nicotinic acetylcholine α4β2 receptor class. In preparation for using this tracer in humans we have performed whole-body PET studies in mice to evaluate the *in vivo* biodistribution and dosimetry of [^{18}F]Nifene.

Methods—Seven BALB/c mice (3 males, 4 females) received IV tail injections of [^{18}F]Nifene and scanned for 2 hours in an Inveon dedicated PET scanner. Each animal also received a high resolution CT scan using an Inveon CT. The CT images were used to draw volume of interest (VOI) on the following organs: brain, large intestine, small intestine, stomach, heart, kidneys, liver, lungs, pancreas, bone, spleen, testes, thymus, uterus and urinary bladder. All organ time activity curves had the decay correction reversed and were normalized to the injected activity. The area under the normalized curves was then used to compute the residence times in each organ. The absorbed doses in mouse organs were computed using the RAdiation Dose Assessment Resource (RADAR) animal models for dose assessment. The residence times in mouse organs were converted to human values using scale factors based on differences between organ and body weights. OLINDA 1.1 software was used to compute the absorbed human doses in multiple organs for both female and male phantoms.

Results—The highest mouse residence times were found in urinary bladder, liver, bone, small intestine and kidneys. The largest doses in mice were found in urinary bladder and kidneys for both females and males. The elimination of radiotracer was primarily via kidney and urinary bladder with the urinary bladder being the limiting organ. The projected human effective doses were 1.51E-02 mSv/MBq for the adult male phantom and 1.65E-02 mSv/MBq for the adult female model phantom.

Conclusion—This study indicates that the whole-body mouse imaging can be used as a preclinical tool for initial estimation of the absorbed doses of [^{18}F]Nifene in humans.

Keywords

[^{18}F]Nifene; α4β2; Biodistribution; Dosimetry; PET; Preclinical

Corresponding Author: Cristian C. Constantinescu, Ph.D., Department Radiological Sciences, University of California Irvine, Medical Sciences B, B-140, Irvine, CA 92697-5000, Phone: +1 949 824 0709, Fax: +1 949 824 2344, constant@uci.edu.

1. Introduction

Nicotinic acetylcholine receptors (nAChRs) and the α4β2 subtype in particular are of interest for imaging and therapeutic applications. They have been a target for continued development of effective PET radioligands as they have been demonstrated to be involved in cognitive processes such as learning, memory, and control of movement in normal subjects. The relevance of α4β2 receptor imaging extends to many CNS disorders such as Alzheimer's disease [1–4], Parkinson's disease [5;6], schizophrenia [7], and nicotine dependence [8;9]. A number of animal model studies have suggested that nicotinic α4β2 receptors have a role in learning and memory [10;11].

PET radiotracers for α4β2 receptors have been developed for human studies. The currently established agonist PET radiotracer for α4β2 receptors in use in humans is 2-[^{18}F]FA-85380 [12]. The main drawback of this radioligand is the long PET acquisition time usually required to achieve transient equilibrium (>5 hours) [13]. [^{18}F]Nifene is being developed as a PET agent with faster kinetics as a potential superior alternative to 2-[^{18}F]FA-85380 for the non-invasive study of nAChRs in the brain.

[^{18}F]Nifene, an analog of 2-[^{18}F]FA-85380, is a highly selective acetylcholine α4β2 receptor radioligand (K_i= 0.50 nM, [14]) that has been shown to reach equilibrium fast and yield moderate specific/non-specific ratios in non-human primates in vivo [15]. Rodent imaging studies using [^{18}F]Nifene have also been reported that showed fast equilibrium and moderate binding in both thalamic and extra thalamic regions [16]. The same studies also found low test-retest variability (3% in the thalamus) and demonstrated displacement by nicotine *in vivo*. The shorter scan time (60 min) required with [^{18}F]Nifene represents an advantage in human studies over other tracers with similar characteristics such as 2-[^{18}F]FA-85380 that require scan times up to 5 hours. The promising characteristics of [^{18}F]Nifene makes this tracer a good candidate for use in humans. In this work we evaluated the *in vivo* biodistribution of [^{18}F]Nifene in the mouse organs using whole-body PET and CT imaging. Residence times were computed for several mouse organs and absorbed doses were then derived using the RAdiation Dose Assessment Resource (RADAR) models for dose assessment developed at Vanderbilt University [17] [18]. The mouse residence times were extrapolated to humans based on simple assumptions on difference between the species. We used OLINDA/EXM dosimetry package to derive human organ doses for both adult female and adult male phantoms based on the projected residence times.

2. Materials and methods

2.1 Tracer Synthesis

[^{18}F]Nifene (or 2-[^{18}F]fluoro-3-[2-((S)-3-pyrrolinyl)methoxy]pyridine) was synthesized as reported in [14]. The automated radiosynthesis of [^{18}F]Nifene was carried out in the chemistry-processing control unit (CPCU) box. An Alltech C_{18} column (10 μm, 250 × 10 mm^2) was used for reverse-phase HPLC purification. The specific activity of [^{18}F]Nifene exceeded 74 MBq/nmol (2 Ci/μmol) at the end of synthesis.

2.2 Subjects

This study was conducted under protocols approved by the Institutional Animal Care and Use Committee of University of California Irvine. Seven BALB\c mice, 3 males and 4 females (23.4 ± 0.98 g), were used for this study. The animals were separated based on gender and housed in cages in a climate controlled room (24.4°C), with a 12:12-hour light cycle. Subjects had free access to food and water during housing. All animals were fasted for 18–24 hours prior to PET imaging. In preparation for the scans, the mice were induced into anesthesia with 4% isoflurane.

2.3 PET and CT scanning

Mice received iv tail injections (7.14 ± 1.79 MBq) of [^{18}F]Nifene off the scanner bed and then were immediately placed in the mouse imaging chamber for PET acquisition and scanned for 120 minutes in an Inveon dedicated PET scanner (Siemens Medical Solutions, Knoxville, TN). The average delay between the time of injection and the start of the scan was 3.9 ± 1.6 min. The animals were maintained under 2% isoflurane anesthesia throughout the scanning period. The PET list-mode data were dynamically histogrammed into 23 3D-sinograms of span 3 and ring difference 79 (4 × 1min, 3 × 2 min, 10 × 5 min, 6 × 10 min). Following Fourier rebinning the images were reconstructed using a 2D ordered-subset expectation maximization (OSEM2D) algorithm (16 subsets, 4 iterations, 2 EM iterations) into 128 × 128 × 159 arrays with a 0.77 mm pixel size and a slice thickness of 0.796 mm. Random events were subtracted prior to reconstruction. Normalization of detector responses was performed using a component based method. All dynamic images were automatically corrected for radioactive decay due to manufacturer software settings. Following the PET acquisition each mouse received a high resolution CT scan with an Inveon Multimodality CT scanner mechanically docked to the Inveon PET without being removed from the scanner bed. The CT scan was performed at 2 overlapping bed positions with detector-source rotating 360 degrees around the animal with projections acquired every 0.5 degrees (720 angles). CT images were reconstructed with a cone beam algorithm (bilinear interpolation, Shepp-Logan filter) into 480 × 480 × 632 image arrays with a 206 μm pixel size. Following the reconstruction the CT images were spatially aligned to match the PET images using a fixed, predetermined transformation matrix. In addition to being reconstructed into an image, the CT data were used for attenuation correction of PET images. Quantitative calibration of PET images was performed by scanning 6.2 MBq of well mixed [^{18}F]Nifene and Millipore water solution inside a 56.5 ml plastic container. The [^{18}F]Nifene activity used in calibration was measured in the same dose calibrator used to measure the activities administered to the subjects.

2.4 Image Analysis

Processing of reconstructed images was performed with PMOD software package (PMOD Technologies). The mouse organs were identified and 3D volumes of interest (VOIs) were manually drawn as irregular contours on the high resolution CT images acquired for each mouse. VOIs were placed on the following “source” organs: brain, lower large intestine, small intestine, stomach, heart, kidneys, liver, lungs, pancreas, bone (femur), spleen, testes (males only), uterus (females only), thymus, and urinary bladder (Fig. 1). The size of each VOI was smaller than the actual size of each organ in order to reduce the PET effects of spill in and spillover from adjacent organs. The VOIs representing the cortical bone were generated by delineating parts of the femur bone. The liver VOI included the gall bladder which could not be clearly identified on either the CT or PET images. All VOIs were transferred to dynamic PET images and the *decay-corrected* mean time activity curves (TACs) were extracted for each target organ.

2.5 Dose calculations

Following the extraction of time activity curves the residence times of radioactive [^{18}F]Nifene in each target organ and the absorbed doses in multiple “source” organs were computed using Matlab. Since in dose calculation the actual activity over time is of interest the decay correction was *reversed* prior to computation of residence times using the formula

$$TAC(t)=TAC_{corr}(t)x\,(\lambda/\Delta t)\,x\,(1-\exp(-\lambda\,\Delta t))\,/\exp(\lambda\,t_s) \quad (1)$$

TAC_{corr} is the decay-corrected TAC, is the decay constant for ^{18}F, Δt is the frame duration, and t_s is the start time of each frame. The residence times R_i in the ith organ was computed using formula

$$R(i)=O_m(i)\times\int_0^\infty TAC(i,t)dt/A_{inj} \quad (2)$$

, where $TAC(i,t)$ is the time activity curve for the ith organ [Bq/cc], $O_m(i)$ is the mass of the ith organ [g], and A_{inj} is the administered activity [Bq]. The organ masses for the 25g mouse model were taken from Table 1 in [17] and divided by the average organ density of 1g/cc before being used in (2). Thus the units for the residence times were [Bq-hr/Bq administered]. The integral in (2) was computed using area under the curve (AUC) for each TAC. The AUC between the time of [^{18}F]Nifene injection and start of the scan was computed assuming linearity. The AUC between the start and the end of the scan was computed numerically using trapezoidal method. The integral between the end of the scan and infinity was computed analytically assuming the kinetics was governed by the radioactive decay of ^{18}F. The residence times for the remainder of the body were computed by subtracting the sum of all organs residence times from the maximum, physically allowed, residence time, which for ^{18}F is equal to 2.62 (= $T_{1/2}$/ln2). The dose absorbed by the ith target organ was computed as:

$$OD(i)=\sum_j R(j)\times DF(j,i) \quad (3)$$

, where $R(j)$ = residence time for the j th organ, $DF(j,i)$ = dose factor between the j th source organ and the i th target organ

The dose factors, which are a function of mouse weight and relate the residence times in source organs to the absorbed dose in each target organ, were taken from Table 3 in [17]. Further, the residence times for humans, $R_{h,}$ were computed from mouse residence times, R_m by using %-kg/g extrapolation, which assumes proportionality based on weight difference between species [19]:

$$R_h=R_m\times(O_h/B_h)/(O_m/B_m) \quad (4)$$

with O_h = human organ weight, O_m = mouse organ weight, B_h = human body weight, B_m = mouse body weight. The human body weight, $B_{h,}$ and the human organ masses, $O_{h,}$ were taken from OLINDA 1.1 for adult female and adult male phantom, respectively. The mouse body weight, B_m, and the mouse organ masses were those of a 25 g mouse in the RADAR model [17]. The projected human doses were then computed for both males and female phantoms using OLINDA 1.1 software package with the human residence times, R_h, as input.

3. Results

The VOI delineation on CT images is illustrated in Fig. 1 that shows two coronal and one sagital views of a male mouse. Figure 2 shows whole body mouse PET images from early (0–30 min) and late (90–120 min) parts of the scan. In the early part of the scan the urinary bladder, and the kidneys presented the highest [^{18}F]Nifene activity, followed by four organs with similar activity, namely the liver, pancreas, spleen and stomach. In the later part (90–120 min) the urinary bladder values were highest, followed by stomach, kidneys and bone.

The stomach activity is slowly increases up to around 90 min followed by a slow decrease toward the end of the scan.

The specificity of [^{18}F]Nifene for α4β2 receptors is illustrated in Fig. 2E, which shows orthogonal PET slices through the brain of one the subjects (average 30–60 min, bottom row) as well as an overlay with an MR template [20] (top row). Thalamus, a brain region rich in α4β2 receptors, presents highest tracer uptake. Representative TACs normalized to the injected activity in source organs are shown in Fig. 3.

Table 1 lists the residence times of [^{18}F]Nifene in all mouse organs. The largest values were found in urinary bladder (in both genders), liver, bone, small intestine and kidneys. The largest absorbed dose was received by the urinary bladder (“limiting organ”) of both male (6.20E+02 ± 2.48E+02 mSv/MBq) and female (9.85E+02 ± 3.24E+02 mSv/MBq) mice (Table 2). The mean residence times for both adult female and male phantoms are listed in Table 3 and the mean projected human doses are listed in Table 4. Urinary bladder received the highest absorbed dose for both male (5.74E-02 ± 1.81E-02 mSv/MBq) and female (9.32E-02 ± 2.63E-02 mSv/MBq) phantoms. The mean effective doses were 1.51E-02 ± 4.04E-04 mSv/MBq (adult male phantom) and 1.65E-02 ± 8.73E-04 mSv/MBq (adult female phantom), respectively.

4. Discussion

Biodistribution and dosimetry studies are conducted before a PET radiotracer is used in humans in order to estimate the internal radiation dose absorbed by each human organ and determine the occurrence and the number of studies that can be safely conducted. The availability of preclinical PET and CT scanners and the existence of physical models for internal dose assessment in small animals allow preliminarily evaluation of tracer biodistribution in mice or rats and the extrapolation to humans. The absorbed radiation doses in mouse organs due to the [^{18}F]Nifene radiotracer have been evaluated in this study using whole-body PET/CT and a mouse model of dose assessment. The mouse data has been extrapolated to humans based on simple assumptions on differences between species.

Elimination of [^{18}F] Nifene from mouse body occurred via urinary system as indicated by the kidney activity preceding the urinary bladder as well as by the much higher activity in the urinary tract than in the digestive system (e.g. stomach, LLI). Urinary bladder was the ‘limiting organ’ with the largest absorbed dose. No voiding urinary bladder model was used in computations of the residence times. Gallbladder and female mouse reproduction organs such as uterus and ovaries are not included in the RADAR model at this time and thus we lumped them with the rest of the body.

Since [^{18}F]Nifene is an analog of 2-[^{18}F]FA-85380 that targets the same class of neuroreceptors we compared the human doses of [^{18}F]Nifene as projected by this study with those from a human dosimetry study with 2-[^{18}F]FA-85380 [21]. Comparisons involved only the male phantom data as in the 2-[^{18}F]FA-85380 study all human subjects were male. The [^{18}F]Nifene doses were similarly ranked and correlated highly ($r = 0.881$, $p < 0.001$) to those of 2-[^{18}F]FA-85380, with urinary bladder and kidney receiving the highest dose in both cases (Fig. 4). The dose values for the two tracers were similar in order of magnitude with the 2-[^{18}F]FA-85380 values generally higher than those of [^{18}F]Nifene. 2-[^{18}F]FA-85380 is the tracer with higher affinity and therefore increased biological half-life in regions with specific binding. However, since most of the uptake of the tracer and its metabolites is nonspecific it is reasonable to believe that differences in specificity contributes insignificantly to differences in dosimetry.

Currently it is not readily accepted that dosimetry estimates can be extrapolated from rodents to humans without validation. Two important factors are to be taken in account when deriving human doses from mouse data: the tracer metabolic rates in the two species and the extrapolation method. For this study we assumed that the metabolic rates were similar in mouse and human. Studies with translocator protein tracers that used the same mass extrapolation method (Eq.(4)) showed that the effective doses calculated from rat data were overestimated compared to those measured in nonhuman primates [22]. On the other hand the results of our previous work [23] in which we extrapolated the mouse dosimetry of the 5-HT_{1A} tracer [^{18}F]Mefway to human suggested that the urinary organs (bladder and kidneys) doses derived from the mouse model were underestimated.

One of the goals of a human dosimetry study is to estimate the maximum activity that can be administered to a human subject without surpassing the dose limits allowed. According to the federal regulations specified in Title 21 CFR 361.1 [24] the radiation doses to the whole body, gonads, active blood-forming organs, and lens of the eye should not exceed 50 mSv (5 rem) annually and 30 mSv (3 rem) for a single study. The dose absorbed by all other organs should not exceed 150 mSv (15 rem) annually and 50mSv (5 rem) per study. According to the present study the urinary bladder is the limiting organ for [^{18}F]Nifene and therefore sets the maximum administered activity per study. Based on our projected human doses for urinary bladder the calculated limits for injected [^{18}F]Nifene activity are 871 MBq (23.5 mCi) for the male model and 536.5 MBq (14.5 mCi) for the adult female model. These values should allow multiple (> 3) studies per year for each subject. An injected activity of 185 MBq (5 mCi) of [^{18}F]Nifene, adequate for a brain study, would yield a limiting dose of 10.6 mSv for an adult male subject, below Title 21 specifications. In comparison, according to International Commission on Radiological Protection (ICRP) Publication 106 the adult limiting dose for [^{18}F]FDG in adults is 0.13 mSv/MBq which translates into 384 MBq (10 mCi) per study.

Although not meant to be a substitute for a complete dose assessment in humans, the current study is a useful preliminary data set as [^{18}F]Nifene is being translated to humans. As a future research we are planning [^{18}F]Nifene dosimetry studies in human subjects that will assist to verify and validate the accuracy of the animal model results presented in this study.

Acknowledgments

The project described was supported by Grant Number NIH R01 AG029479 from the National Institute of Aging (NIA) awarded to Jogeshwar Mukherjee.

References

1. Wu J, Ishikawa M, Zhang J, Hashimoto K. Brain imaging of nicotinic receptors in Alzheimer's disease. Int J Alzheimers Dis. 2010; 2010:548913. [PubMed: 21253523]
2. Kendziorra K, Wolf H, Meyer PM, Barthel H, Hesse S, Becker GA, Luthardt J, Schildan A, Patt M, Sorger D, Seese A, Gertz HJ, Sabri O. Decreased cerebral alpha4beta2* nicotinic acetylcholine receptor availability in patients with mild cognitive impairment and Alzheimer's disease assessed with positron emission tomography. Eur J Nucl Med Mol Imaging. 2011; 38:515–525. [PubMed: 21069319]
3. Kadir A, Almkvist O, Wall A, Langstrom B, Nordberg A. PET imaging of cortical 11C-nicotine binding correlates with the cognitive function of attention in Alzheimer's disease. Psychopharmacology (Berl). 2006; 188:509–520. [PubMed: 16832659]
4. Sihver W, Langstrom B, Nordberg A. Ligands for in vivo imaging of nicotinic receptor subtypes in Alzheimer brain. Acta Neurol Scand Suppl. 2000; 176:27–33. [PubMed: 11261802]

5. Valette H, Bottlaender M, Dolle F, Guenther I, Fuseau C, Coulon C, Ottaviani M, Crouzel C. Imaging central nicotinic acetylcholine receptors in baboons with [18F]fluoro-A-85380. J Nucl Med. 1999; 40:1374–1380. [PubMed: 10450691]
6. Bucerius J, Joe AY, Schmaljohann J, Gundisch D, Minnerop M, Biersack HJ, Wullner U, Reinhardt MJ. Feasibility of 2-deoxy-2-[18F]fluoro-D-glucose- A85380-PET for imaging of human cardiac nicotinic acetylcholine receptors in vivo. Clin Res Cardiol. 2006; 95:105–109. [PubMed: 16598519]
7. Brasic JR, Cascella N, Kumar A, Zhou Y, Hilton J, Raymont V, Crabb A, Guevara MR, Horti AG, Wong DF. Positron emission tomography experience with 2-[(1)F]fluoro-3-(2(S)-azetidinylmethoxy)pyridine (2-[(1)F]FA) in the living human brain of smokers with paranoid schizophrenia. Synapse. 2012; 66:352–368. [PubMed: 22169936]
8. Le Foll B, Chefer SI, Kimes AS, Shumway D, Stein EA, Mukhin AG, Goldberg SR. Baseline expression of alpha4beta2* nicotinic acetylcholine receptors predicts motivation to self-administer nicotine. Biol Psychiatry. Apr 15.2009 65:714–716. [PubMed: 19095220]
9. Mukhin AG, Kimes AS, Chefer SI, Matochik JA, Contoreggi CS, Horti AG, Vaupel DB, Pavlova O, Stein EA. Greater nicotinic acetylcholine receptor density in smokers than in nonsmokers: a PET study with 2-18F-FA-85380. J Nucl Med. 2008; 49:1628–1635. [PubMed: 18794265]
10. Li JG, Lehr M, Liu-Chen LY, Woodruff-Pak DS. Nicotinic acetylcholine receptors and modulation of learning in 4- and 27-month-old rabbits. Neuropsychopharmacology. 2008; 33:2820–2830. [PubMed: 18256594]
11. Bieszczad KM, Kant R, Constantinescu CC, Pandey SK, Kawai HD, Metherate R, Weinberger NM, Mukherjee J. Nicotinic acetylcholine receptors in rat forebrain that bind (18) F-nifene: Relating PET imaging, autoradiography, and behavior. Synapse. 2012; 66:418–434. [PubMed: 22213342]
12. Horti AG, Scheffel U, Koren AO, Ravert HT, Mathews WB, Musachio JL, Finley PA, London ED, Dannals RF. 2-[18F]Fluoro-A-85380, an in vivo tracer for the nicotinic acetylcholine receptors. Nucl Med Biol. 1998; 25:599–603. [PubMed: 9804040]
13. Vaupel DB, Stein EA, Mukhin AG. Quantification of alpha4beta2* nicotinic receptors in the rat brain with microPET and 2-[18F]F-A-85380. Neuroimage. Feb 15.2007 34:1352–1362. [PubMed: 17187994]
14. Pichika R, Easwaramoorthy B, Collins D, Christian BT, Shi B, Narayanan TK, Potkin SG, Mukherjee J. Nicotinic alpha4beta2 receptor imaging agents: part II. Synthesis and biological evaluation of 2-[18F]fluoro-3-[2-((S)-3-pyrrolinyl)methoxy]pyridine (18F-nifene) in rodents and imaging by PET in nonhuman primate. Nucl Med Biol. 2006; 33:295–304. [PubMed: 16631077]
15. Hillmer AT, Wooten DW, Moirano JM, Slesarev M, Barnhart TE, Engle JW, Nickles RJ, Murali D, Schneider ML, Mukherjee J, Christian BT. Specific alpha4beta2 nicotinic acetylcholine receptor binding of [F-18]nifene in the rhesus monkey. Synapse. 2011; 65:1309–1318. [PubMed: 21674627]
16. Kant R, Constantinescu CC, Parekh P, Pandey SK, Pan ML, Easwaramoorthy B, Mukherjee J. Evaluation of F-nifene binding to alpha4beta2 nicotinic receptors in the rat brain using microPET imaging. EJNMMI Res. 2011:1, 6.
17. Keenan MA, Stabin MG, Segars WP, Fernald MJ. RADAR realistic animal model series for dose assessment. J Nucl Med. 2010; 51:471–476. [PubMed: 20197451]
18. Stabin MG, Sharkey RM, Siegel JA. RADAR commentary: Evolution and current status of dosimetry in nuclear medicine. J Nucl Med. 2011; 52:1156–1161. [PubMed: 21680699]
19. Kirschner AS, Ice RD, Beierwaltes WH. Radiation-Dosimetry of I-131-19-Iodocholesterol - Pitfalls of Using Tissue Concentration Data - Reply. Journal of Nuclear Medicine. 1975; 16:248–249.
20. Ma Y, Smith D, Hof PR, Foerster B, Hamilton S, Blackband SJ, Yu M, Benveniste H. In Vivo 3D Digital Atlas Database of the Adult C57BL/6J Mouse Brain by Magnetic Resonance Microscopy. Front Neuroanat. 2008; 2:1. [PubMed: 18958199]
21. Bottlaender M, Valette H, Roumenov D, Dolle F, Coulon C, Ottaviani M, Hinnen F, Ricard M. Biodistribution and radiation dosimetry of 18F-fluoro-A-85380 in healthy volunteers. J Nucl Med. 2003; 44:596–601. [PubMed: 12679405]

22. Verschuer JD, Towson J, Eberl S, Katsifis A, Henderson D, Lam P, Wen L, Loc'h C, Mattner F, Thomson S, Mohamed A, Fulham MJ. Radiation dosimetry of the translocator protein ligands [18F]PBR111 and [18F]PBR102. Nucl Med Biol. 2012; 39:742–753. [PubMed: 22300959]

23. Constantinescu CC, Sevrioukov E, Garcia A, Pan M-L, Mukherjee J. Evaluation of [^{18}F]Mefway biodistribution and dosimetry based on whole-body PET imaging of mice. Mol Imaging Biol. 2012 Jul 26. [Epub ahead of print].

24. Food and Drug Administration. Title 21 CFR 361.1 Radioactive Drugs for Certain Research Uses. Washington DC: National Archives and Records Administration, Office of the Federal Register; 2011. p. 325-330.

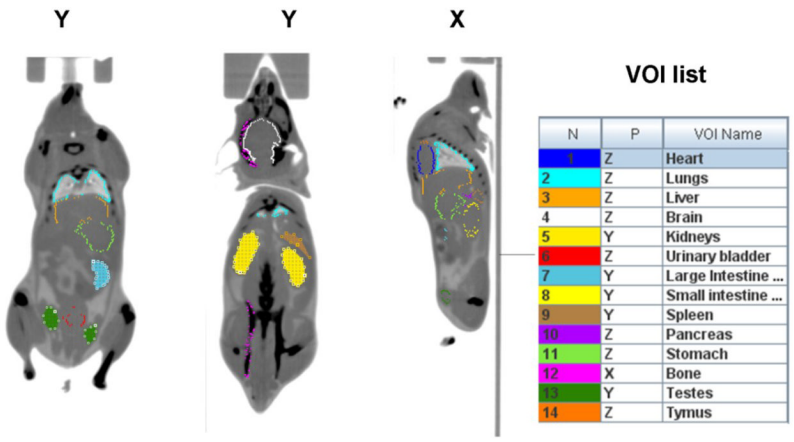

Fig. 1.

Representative mouse CT images in coronal (Y) and sagital (X) views showing the drawing of volume of interest (VOIs) on different organs. The CT images were acquired at 2 overlapping bed positions. The VOIs drawn in the same view as the one shown appear as filled contours while the ones drawn in different view appear as colored contours. The complete list of VOIs is shown on the right hand side.

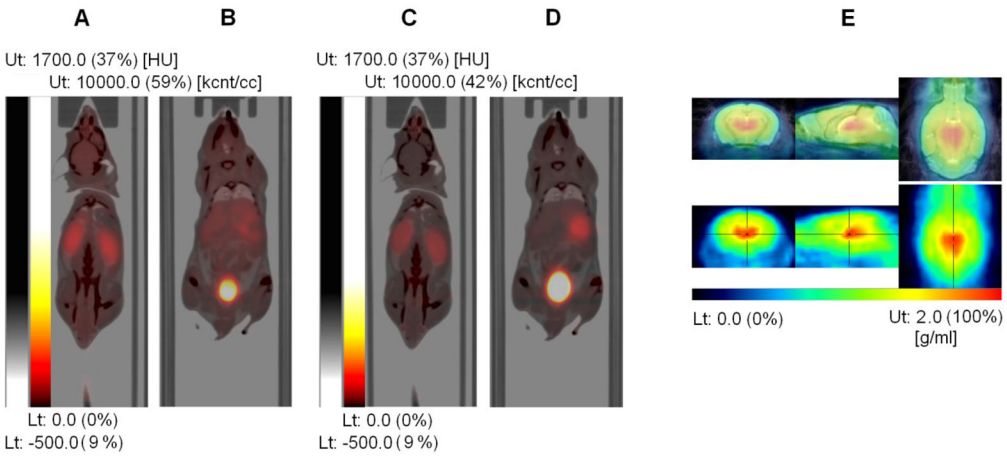

Fig. 2.

Fused PET and CT images with PET images from the first 30 min (**A**, **B**) and from 90 to 120 min (C, D) after injection of [^{18}F]Nifene (weighted summation of dynamic frames). The early image (**A**) shows higher tracer uptake in the kidney compared with the late images (C) while the late image (**D**) shows higher tracer uptake in the urinary bladder than the early image (**B**). This illustrates that the elimination of the tracer from mouse body occurs primarily via urinary system. (**E**) PET images (30–60 min) of the mouse brain (bottom row) showing high selective binding of [^{18}F]Nifene in the thalamus (marked with orthogonal crosshairs), a region rich in α4β2 receptors. Images were co-registered to an MR mouse brain template (top panel, fused image).

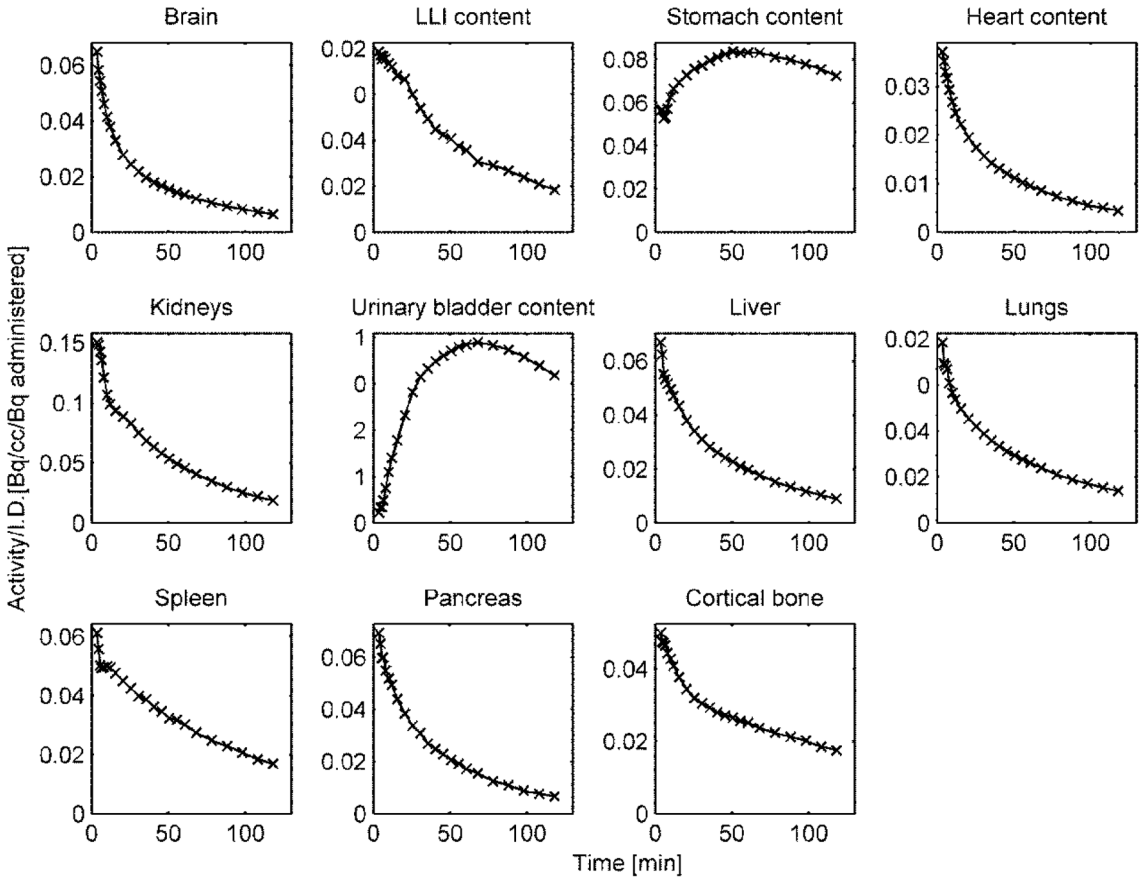

Fig. 3.

Representative [^{18}F]Nifene time activity curves (not decay corrected) normalized to the injected activity from multiple mouse (male) organs. The integral under the curve between injection and start of the scan was calculated using linear extrapolation of pre-peak data points. The integral under the curve between end of the scan and infinity was computed using exponential extrapolation and assuming kinetics were dictated by the radioactive decay.

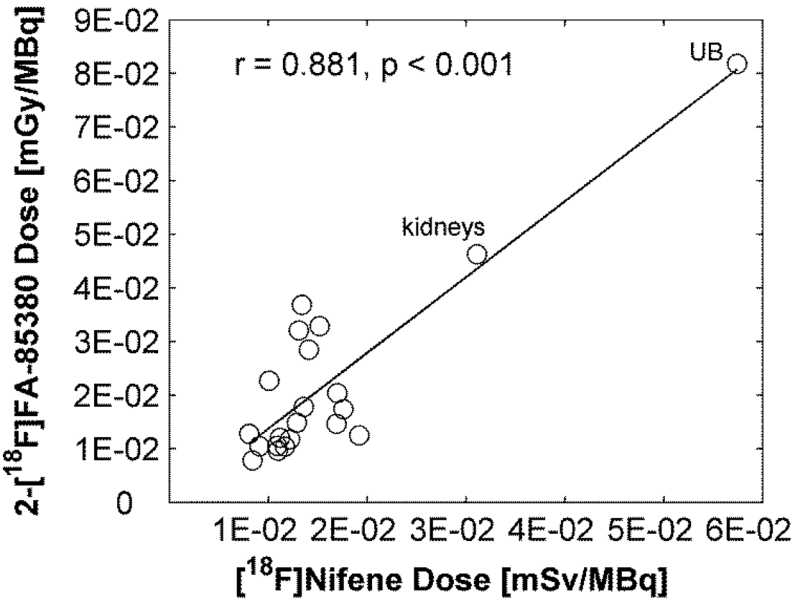

Fig. 4.

Comparison of radiation dose estimate from an *in vivo* human PET study with 2-[^{18}F]FA-85380 (values taken from [21], Table 3) and human doses of [^{18}F]Nifene as projected by this study. Solid line represents the linear regression. Correlation coefficient and the p values are shown on the plot. The data points corresponding to the urinary bladder (UB) and kidneys are labeled. Note: The units are different between the axes. However, since the radiation exposure is from beta particles and gamma-rays, which have a biological effectiveness factor of 1, one may assume that Gy=Sv.

Table 1

Residence times (in Bq-hr/Bq administered) of [^{18}F]Nifene in mouse organs.

Source Organ	Male average (± SD)	Female average (± SD)
Brain	2.88E-02 ± 4.12E-03	2.91E-02 ± 1.80E-03
LLI Content*	2.56E-02 ± 1.02E-02	3.51E-02 ± 1.05E-02
SI Content*	7.80E-02 ± 3.08E-02	1.19E-01 ± 1.94E-02
Stomach Content	1.73E-02 ± 9.66E-03	1.64E-02 ± 4.59E-03
Heart Content	9.71E-03 ± 1.38E-03	9.33E-03 ± 7.20E-04
Kidneys	1.00E-01 ± 5.03E-02	6.21E-02 ± 1.09E-02
Liver	1.56E-01 ± 4.12E-02	1.58E-01 ± 1.13E-02
Lungs	4.32E-03 ± 1.32E-04	3.31E-03 ± 3.59E-04
Pancreas	3.56E-02 ± 1.65E-02	3.67E-02 ± 1.03E-02
Cortical Bone	1.57E-01 ± 5.11E-02	1.11E-01 ± 3.21E-02
Spleen	1.47E-02 ± 4.24E-03	1.31E-02 ± 2.97E-03
Testes	1.22E-02 ± 8.49E-03	N/A
Thymus	6.39E-04 ± 1.44E-04	7.11E-04 ± 6.81E-05
UB Content*	2.99E-01 ± 1.23E-01	4.82E-01 ± 1.57E-01
Uterus	N/A	4.67E-03 ± 1.67E-03
Remainder Body	1.70E+00 ± 1.31E-01	1.56E+00 ± 1.76E-01

LLI = lower large intestine, SI = small intestine, UB = urinary bladder

Table 2

Absorbed mouse organ doses (in mSv/MBq) for [^{18}F]Nifene.

Target Organ	Male average (± SD)	Female average (± SD)
Brain	2.02E+01 ± 1.84E+00	1.93E+01 ± 8.94E-01
LLI Wall*	1.89E+01 ± 1.58E+00	2.04E+01 ± 2.60E+00
Small Intestine	1.90E+01 ± 1.54E+00	2.15E+01 ± 1.01E+00
Stomach Wall	3.98E+01 ± 1.32E+01	3.75E+01 ± 5.70E+00
Heart Wall	1.85E+01 ± 1.38E+00	1.73E+01 ± 1.20E+00
Kidneys	5.60E+01 ± 2.24E+01	3.89E+01 ± 4.99E+00
Liver	2.54E+01 ± 3.58E+00	2.46E+01 ± 1.90E+00
Lungs	1.93E+01 ± 4.69E-01	1.69E+01 ± 9.62E-01
Pancreas	2.89E+01 ± 7.78E+00	2.84E+01 ± 4.02E+00
Osteogenic Cells	1.75E+01 ± 2.10E+00	1.43E+01 ± 1.41E+00
Spleen	2.98E+01 ± 5.90E+00	2.73E+01 ± 2.42E+00
Testes	2.26E+01 ± 6.49E+00	N/A
Thyroid	1.78E+01 ± 1.14E+00	1.72E+01 ± 1.11E+00
UB Wall*	6.20E+02 ± 2.48E+02	9.85E+02 ± 3.24E+02
Total Body	1.71E+01 ± 3.62E-02	1.71E+01 ± 7.99E-02

LLI = lower large intestine, UB = urinary bladder

Table 3

Human residence times (in Bq-hr/Bq administered) estimates of [^{18}F]Nifene based on mouse residence times and modeled organ mass differences between the two species.

Source Organ	Male average (± SD)	Female average (± SD)
Brain	3.58E-02 ± 5.11E-03	3.30E-02 ± 2.03E-03
LLI Content*	2.98E-03 ± 1.19E-03	4.24E-03 ± 1.27E-03
SI Content*	4.01E-03 ± 1.59E-03	6.00E-03 ± 9.80E-04
Stomach Content	2.03E-02 ± 1.13E-02	1.83E-02 ± 5.13E-03
Heart Content	5.32E-03 ± 7.57E-04	4.19E-03 ± 3.23E-04
Kidneys	4.05E-02 ± 2.03E-02	2.49E-02 ± 4.38E-03
Liver	6.96E-02 ± 1.84E-02	5.59E-02 ± 3.99E-03
Lungs	2.02E-02 ± 6.19E-04	1.34E-02 ± 1.45E-03
Pancreas	4.48E-03 ± 2.07E-03	4.50E-03 ± 1.27E-03
Cortical Bone	3.28E-02 ± 1.07E-02	2.91E-02 ± 8.41E-03
Spleen	9.88E-03 ± 2.85E-03	7.78E-03 ± 1.77E-03
Testes	1.21E-03 ± 8.44E-04	N/A
Thymus	3.89E-04 ± 8.77E-05	4.47E-04 ± 4.27E-05
UB Content*	9.67E-02 ± 3.97E-02	1.27E-01 ± 4.13E-02
Uterus	N/A	4.68E-03 ± 1.67E-03
Remainder Body	2.12E+00 ± 1.63E-01	1.62E+00 ± 1.82E-01

LLI = lower large intestine, SI = small intestine, UB = urinary bladder

Table 4

Human doses (in mSv/MBq) estimates for [^{18}F]Nifene generated with OLINDA 1.1 software using residence times estimated from the mouse residence times.

Target Organ	Male average (± SD)	Female average (± SD)
Adrenals	1.29E-02 ± 1.26E-03	1.25E-02 ± 1.15E-03
Brain	8.09E-03 ± 9.55E-04	8.52E-03 ± 2.86E-04
Breasts	8.85E-03 ± 6.47E-04	8.63E-03 ± 9.10E-04
Gallbladder Wall	1.36E-02 ± 1.10E-03	1.25E-02 ± 1.07E-03
LLI Wall*	1.52E-02 ± 6.00E-04	1.65E-02 ± 1.09E-03
Small Intestine	1.41E-02 ± 4.58E-04	1.33E-02 ± 7.30E-04
Stomach Wall	1.92E-02 ± 3.56E-03	1.89E-02 ± 1.38E-03
ULI Wall*	1.31E-02 ± 8.02E-04	1.30E-02 ± 1.03E-03
Heart Wall	1.22E-02 ± 9.17E-04	1.17E-02 ± 1.02E-03
Kidneys	3.11E-02 ± 1.27E-02	2.26E-02 ± 3.03E-03
Liver	1.34E-02 ± 2.41E-03	1.38E-02 ± 9.75E-04
Lungs	9.12E-03 ± 5.14E-04	8.46E-03 ± 4.64E-04
Muscle	1.09E-02 ± 6.66E-04	1.05E-02 ± 8.91E-04
Ovaries	NA	1.44E-02 ± 6.65E-04
Pancreas	1.69E-02 ± 4.38E-03	1.73E-02 ± 2.44E-03
Red Marrow	1.01E-02 ± 6.66E-04	9.73E-03 ± 8.63E-04
Osteogenic Cells	1.76E-02 ± 6.93E-04	1.70E-02 ± 3.21E-03
Skin	8.43E-03 ± 5.82E-04	8.10E-03 ± 7.98E-04
Spleen	1.70E-02 ± 3.44E-03	1.61E-02 ± 1.82E-03
Testes	1.17E-02 ± 3.43E-03	NA
Thymus	9.15E-03 ± 7.82E-04	9.60E-03 ± 5.97E-04
Thyroid	1.10E-02 ± 8.62E-04	9.80E-03 ± 1.07E-03
UB Wall*	5.74E-02 ± 1.81E-02	9.32E-02 ± 2.63E-02
Uterus	NA	2.15E-02 ± 3.14E-03
Total Body	1.12E-02 ± 7.00E-04	1.10E-02 ± 8.85E-04
Effective dose equivalent	1.68E-02 ± 2.65E-04	1.83E-02 ± 9.74E-04
Effective dose	1.51E-02 ± 4.04E-04	1.65E-02 ± 8.73E-04

LLI = lower large intestine, ULI = upper large intestine, UB = urinary bladder